Quantifying Heartbeat Micro-Fragmentations Post-Myocardial Infarction Using Wavelet Entropy and Complexity

Gisela V. Clemente[a,c,*], Leandro Andrini[b,c], Mariano Llamedo Soria[a]

[a]*Departamento de Ingenier´ıa Electro´nica, Facultad Regional Buenos Aires, Universidad Tecnolo´gica Nacional. Grupo de Investigacio´n y Desarrollo en Bioingenier´ıa (GIBIO).*
[b]*Centro de Matema´tica de La Plata (CMaLP), Departamento de Matema´tica, Facultad de Ciencias Exactas, Universidad Nacional de La Plata.*
[c]*CONICET*

Abstract

Cardiovascular diseases are recognized as one of the leading causes of mortality, with myocardial infarction (MI) being a critical condition that disrupts the heart's electrical conduction due to myocardial tissue damage. The aim of this study is to examine two key phases following MI, excluding ventricular tachycardia (VT) and/or ventricular fibrillation (VF): the healing phase (up to one week after, referred to as MI_7) and the healed phase (more than two months after, referred to as MI_{60}). During these phases, severe complications, such as sudden cardiac death, may occur. Electrocardiograms (ECGs) of healthy individuals (C_{TRL}) and MI patients in the MI_7 and MI_{60} stages were analyzed, using data from the PTB and PTB XL databases. The analysis specifically examined the presence of heartbeat micro-fragmentations, known as *µf QRS*, associated with MI, and employed indicators based on Shannon wavelet entropy (H) and Statistical Complexity (C), derived from Continuous Wavelet Transform. Receiver Operating Characteristic (ROC) curves were used to assess these indicators, yielding significant results validated across the databases and their combination. Entropy and Complexity indicators proved to be promising tools for evaluating morphological changes in the heartbeats of post-MI patients. The findings support the usefulness of these indicators in *µf QRS* analysis and highlight their potential application in both clinical and medical research settings.

*Corresponding author
Email address: gclemente@mate.unlp.edu.ar (Gisela V. Clemente)

Preprint not peer reviewed

This preprint research paper has not been peer reviewed. Electronic copy available at: https://ssrn.com/abstract=5349412

Keywords: Heartbeat micro-fragmentations, Wavelet Entropy, Statistical Complexity, Myocardial infarction.

1. Introduction

Myocardial infarction (MI) is a leading cause of malignant ventricular arrhythmias and sudden cardiac death (SCD) due to the electrical disturbances it causes in the heart [1, 2]. Damage during MI leads to conduction abnormalities, particularly during the healing (MI_7) and healed (MI_{60}) stages, which increase the risk of arrhythmias, including sustained ventricular tachycardia and SCD.

The QRS complex, which reflects the synchronized activation of the heart muscle during depolarization, is significantly affected by electrical disruptions after MI. Alterations in normal QRS patterns are caused by delayed or unstable electrical activity, with fragmentation of the QRS complex (fQRS) being a key manifestation of these changes. Some of the fQRS can be visually detected and are known as macro-fragmentations (*Mf QRS*), typically offering a binary classification. However, there may be others that remain hidden and undetected in standard ECG analysis, which are known as micro-fragmentations (*μf QRS*). These *μf QRS* have recently been recognized as poor prognosis independent predictors, indicating that even small alterations in the QRS pattern are associated with significant cardiac risks [3].

In order to identify MI from multi-lead ECG, Xiong et al. [4] proposed strategies focused on deep learning approaches. Specifically, Tadesse et al. [5] focus on ECG signal analysis for non-invasive MI diagnosis and employ a deep learning model based on the fusion of multiple ECG leads to identify MI.

Hnatkova et al. [3, 6] showed that *μf QRS* strongly predicts mortality, outperforming traditional indices such as *Mf QRS* and QRS duration in multivariable analyses. These findings suggest *μf QRS* captures significant electrophysiologic abnormalities that enhance its predictive value. A signal processing technique based on singular value decomposition was introduced, which projects ECG leads into optimized three-dimensional spaces, reconstructs the signals, and quantifies the difference (*μf QRS*) between the original and the reconstructed signals. Furthermore, the indices proposed in a previous work [7], based on Shannon entropy and statistical complexity, aim to enhance the detection of *μf QRS* in post-MI patients. Works based on similar quantifiers have been applied to the spatio-temporal anal-

Preprint not peer reviewed

This preprint research paper has not been peer reviewed. Electronic copy available at: https://ssrn.com/abstract=5349412

ysis of ECG dynamics during acute myocardial ischemia, allowing for the differentiation of behavioral patterns during artery occlusion and recovery [8].

This work employs an analytical method based on wavelet transform and Information Theory to extract relevant features from ECGs of post-MI patients at stages MI_7 and MI_{60}. The goal is to identify *μf QRS*, which reflect changes in electrical activity that may indicate instability and an increased risk of malignant arrhythmias or SCD. A wavelet transform-based method was developed and applied to analyze the QRS complex in these ECGs. Additionally, the generalization capability of the methodology presented in [7] is evaluated on a larger dataset, and the performance of the entropy and complexity quantifiers, defined in Section 2.3, is analyzed.

2. Materials and methods

2.1. ECG databases

In this work, the PTB XL database was incorporated in addition to the original open-source PhysioBank PTB database as in [7]. Both databases were developed by the same institution, the *Physikalisch-Technische Bundesanstalt* (PTB) and are freely available through PhysioNet. These databases do not share any records. The PTB-XL database is much larger than the PTB, as it contains 21,837 ECG records from 18,885 patients, with a fixed duration of 10 seconds and a sampling frequency of 500 Hz. PTB-XL contributes the majority of patients, with 99.18 % in the C_{TRL} group and 86.15 % in MI_{60}, while PTB represents a smaller proportion, particularly in the C_{TRL} group (0.82 %), as can be observed in Table 1. By combining both databases, called *Total*, a larger and more representative sample is obtained, improving the robustness and statistical validity of the results, especially in groups with fewer patients in PTB. This integration allows for better generalization and a more comprehensive view of the different groups. Table 1 presents the number of patients and their proportions relative to the *Total* database for C_{TRL}, MI_7, and MI_{60}, as defined in [7], across each of the databases analyzed. In the PTB database, patients in MI_{60} are included in MI_7, meaning they were followed over time; whereas in the PTB-XL database, MI_7 and MI_{60} do not share any patients.

Preprint not peer reviewed

This preprint research paper has not been peer reviewed. Electronic copy available at: https://ssrn.com/abstract=5349412

Characteristics	C_{TRL}	MI_7	MI_{60}
Patients (n)	48	84	41
	5839	29	255
	5887	113	296
Patients (%)	0.82	74.34	13.85
	99.18	25.66	86.15
Sex (male)	37 (77%)	65 (77%)	33 (80%)
	2471 (42%)	17 (58%)	121 (47%)
	2508 (43%)	82 (73%) †	154 (52%) †, §
Age (mean ± SD)	44 ± 14	59 ± 10 †	55 ± 10 †
	51 ± 17	66 ± 15 †	67 ± 11 †
	51 ± 17	61 ± 12 †	66 ± 12 †, §

Table 1: Summary of patient characteristics (number of patients (n), their proportions relative to the *Total* (%), the distribution of patients by sex (n, %) and age (mean ± SD)) for the C_{TRL}, MI_7, and MI_{60} groups across the studied databases. For each characteristic, the first row corresponds to the PTB database, the second row to the PTB-XL database, and the third row represents the *Total* database. † $p < 0.005$ versus C_{TRL}; § $p < 0.005$ versus MI_7.

2.2. ECG pre-processing

Before the algorithm proposed in [7] was applied, all ECG records underwent a pre-processing step. Initially, a second-order Butterworth notch filter (50 Hz) was applied to eliminate power-line interference. Subsequently, a cubic spline interpolation filter was used to correct for baseline drift and respiratory artifacts caused by variations in skin-electrode impedance [9].

For each subject, R-waves and the corresponding QRS endpoints were identified using a wavelet-based ECG delineation algorithm [10] on lead II. A 256 ms window, centered on each R-wave, was used to capture the entire QRS complex. A QRS template was generated by calculating the median of all detected QRS complexes. The cross-correlation coefficient was computed between the template and each individual QRS complex. If the coefficient exceeded 98%, the corresponding QRS complex was corrected for jitter as in the Woody algorithm [9]; otherwise, it was excluded. Finally, for each of the $n = 1, \ldots, N$ windows of lead II, the QRS complexes were defined to capture at all leads. V_{RMS} noise voltage level was calculated in a window of 20 ms before the Q-point of each beat. QRS complexes with a $V_{RMS} > 20\,\mu V$ were excluded from further analysis.

Preprint not peer reviewed

This preprint research paper has not been peer reviewed. Electronic copy available at: https://ssrn.com/abstract=5349412

2.3. Wavelet entropy and complexity

The *continuous wavelet transform* (CWT) of a signal $s(t) \in L^2(\mathbb{R})$ is expressed as:

$$W_\psi s(a, b) = \langle s, \psi_{a,b} \rangle = \int_{-\infty}^{\infty} s(t)\overline{\psi_{a,b}(t)}\, dt \qquad a, b \in \mathbb{R}, a = 0 \qquad (1)$$

where ψ is the *mother wavelet*, and a and b represent the scale and translation parameters, respectively. In practice, the CWT is computed by discretizing a and b into j and k, respectively. In this way, the wavelet coefficients $c_j(k)$ are obtained [11].

The *wavelet energy* at each scale j is defined as

$$E_j = \sum_{k=0}^{K-1} |c_j(k)|^2$$

and the *Total* wavelet energy is

$$E_{\text{tot}} = \sum_j E_j.$$

The *relative wavelet energy* is then given by

$$\rho_j = E_j / E_{\text{tot}}.$$

The values ρ_j at different scales j represent the probability distribution P of the energy. Using these ρ_j, the *Shannon wavelet entropy* is defined as

$$\mathrm{S}[P] = -\sum_j \rho_j \ln(\rho_j).$$

The *Normalized Wavelet Entropy* is calculated as:

$$\mathrm{H}[P] = \mathrm{S}[P] / \mathrm{S}_{\max}, \qquad (2)$$

where $\mathrm{S}_{\max} = \ln(J)$, with J being the number of scales.

The *Wavelet Statistical Complexity* $\mathrm{C}[P]$ is defined as

$$\mathrm{C}[P] = \mathrm{Q}[P]\, \mathrm{H}[P], \qquad (3)$$

where

Preprint not peer reviewed

This preprint research paper has not been peer reviewed. Electronic copy available at: https://ssrn.com/abstract=5349412

$$Q[P] = Q_0\, D[P, P_e] \qquad 0 \le Q \le 1 \tag{4}$$

represents the *disequilibrium distance*, with Q_0 being a normalization constant and D denoting the distance measure defined by Jensen's divergence [12]. It is well known that $C[P]$ measures the degree of correlation between structures; and that for a given value of $H[P]$, there exists a range of possible values of $C[P]$, ranging from a minimum value C_{min}, to a maximum value C_{max}, of $C[P]$.

Daubechies wavelets of order 6 were selected to enable the comparison with the results in [7]. The first 16 scales were chosen as they cover a frequency range of 32–500 Hz, which includes the high-frequency components relevant for detecting *μf QRS*. Since the QRS complexes from the PTB XL database were sampled at 500 Hz, they were resampled to 1000 Hz in order to apply the same methodology as in [7]. Then, for each scale, the relative wavelet energy was computed, and the quantifiers $H(n)$ and $C(n)$ were calculated using Eqs. (2-3), respectively.

Finally, to obtain single quantifiers, the mean values

$$\bar{H} = \frac{1}{N}\sum_{n=1}^{N} H(n) \qquad \bar{C} = \frac{1}{N}\sum_{n=1}^{N} C(n) \tag{5}$$

were calculated for each lead and patient. Additionally, the multi-lead index proposed in [7] was applied:

$$\bar{H}_{ML} = \sqrt{\frac{1}{L}\sum_{l=1}^{L} \bar{H}_l^2} \tag{6}$$

where l represents the l-th lead, and L is the total number of ECG leads for patients. Similar calculations were performed for wavelet statistical complexity, resulting in the computation of $\bar{C}_{ML}$ in each case.

2.4. Statistical analysis

First, the demographic information provided in each database was analyzed. To do this, Chi-square test analyses were conducted to evaluate sex distribution among the $C_{T\,RL}$, MI_7, and MI_{60} groups in the PTB, PTB-XL, and *total* databases. Furthermore, the following tests were applied to determine whether age differentiates the $C_{T\,RL}$, MI_7, and MI_{60} groups in the PTB, PTB-XL and *total* databases. A normality test (Shapiro-Wilk) was

Preprint not peer reviewed

This preprint research paper has not been peer reviewed. Electronic copy available at: https://ssrn.com/abstract=5349412

performed for each group. If the p-value was less than 0.05, the null hypothesis of normality was rejected, and non-parametric tests were applied. For groups where the data followed a normal distribution, a parametric ANOVA was conducted to compare the three groups. If the ANOVA p-value was significant, post hoc comparisons were carried out using Tukey's test. In the case of non-normal data, the Kruskal-Wallis test was used to compare the groups, followed by pairwise Mann-Whitney U tests if significant differences were found.

After preprocessing the databases, we made statistical comparisons using the indices $\overline{\mathrm{H}}_{\mathrm{ML}}$, $\overline{\mathrm{C}}_{\mathrm{ML}}$ and $\overline{\mathrm{HC}}_{\mathrm{ML}}$ defined in the previous section. In order to evaluate the classification performance, K-fold cross-validation was used, where the datasets were randomly divided into K=10 folds, with each fold serving as a test set once. The final performance was calculated as the mean of the performance measures obtained from each fold, ensuring that heartbeats from the same patient never appears in both training and test sets.

Both indices, $\overline{\mathrm{H}}$ and $\overline{\mathrm{C}}$, for the $\mathrm{C}_{T\,RL}$, MI_7, and MI_{60} groups, for each ECG lead, were calculated and statistically analyzed. First, in order to check if the groups were normally distributed, a D'Agostino-Pearson normality test was applied to the database. Accordingly, nonparametric tests were used to analyze the groups. The Kruskal-Wallis test was then applied to determine whether there were any statistically significant differences in at least one group compared to the others. Post hoc pairwise comparisons were conducted using the Mann-Whitney U test with Bonferroni correction to adjust for multiple comparisons.

Additionally, the multivariate permutation test was computed to analyze statistical significance differences in at least one group with respect to the others when the $\overline{\mathrm{HC}}_{\mathrm{ML}}$ plane was considered, specifically for the ML criterion. Post hoc analyses were performed with appropriate adjustments for multiple comparisons to identify pairwise differences.

To evaluate the statistical performance of the quantifiers proposed, the receiver operating characteristic (ROC) curve was computed by taking the groups two at a time and comparing them. The ROC curve was used as a binary classifier system to obtain the highest possible values of sensitivity and specificity for $\overline{\mathrm{H}}_{\mathrm{ML}}$, $\overline{\mathrm{C}}_{\mathrm{ML}}$, and the $\overline{\mathrm{HC}}_{\mathrm{ML}}$ plane. The area under the curve (AUC) was also computed to evaluate the goodness of the test. All results were expressed as mean ± standard deviation (SD). For all statistical analyses, when the p-value was < 0.05, the differences were considered statistically significant.

Preprint not peer reviewed

This preprint research paper has not been peer reviewed. Electronic copy available at: https://ssrn.com/abstract=5349412

3. Results

The available data from the patients in the different databases were analyzed. Table 1 shows that the MI_7 group is predominantly male, whereas in MI_{60}, the gender difference is not as pronounced. Patients with MI in both groups are significantly older than the controls, with statistically significant differences. Individually, the PTB database did not show differences in sex distribution between groups (p-value = 0.8175), nor did the PTB-XL database (p-value = 0.0564). However, when combining the two databases, there are more men than women in MI_7 and MI_{60} than in C_{TRL}, i.e. the differences in sex distribution became highly significant (p-value = 9.7e-11).

In Figure 1, panel A., the pair $\overline{H}_{ML}$ and $\overline{C}_{ML}$ represented in the $\overline{HC}_{ML}$ plane for the patients of each group, for both the PTB and PTB XL databases. It can be observed that the values of $\overline{H}_{ML}$ and $\overline{C}_{ML}$ coincide in the C_{TRL} group, both in the PTB and PTB XL databases, which can be considered as reference values for these indices in the healthy patient group. In the PTB XL database, the $\overline{HC}_{ML}$ plane shows statistically significant differences between all groups, including between MI_7 and MI_{60}, unlike the PTB database, where this does not occur. Although the proposed indicators were statistically significant for differentiating the groups, increases of the same magnitude and direction were not observed across the groups in any of the two databases. When the *Total* database is considered, the different groups occupy distinct regions of the plane, as shown in Figure 1, panel B. The results are similar to those shown in panel A. for the PTB XL database.

Preprint not peer reviewed

This preprint research paper has not been peer reviewed. Electronic copy available at: https://ssrn.com/abstract=5349412

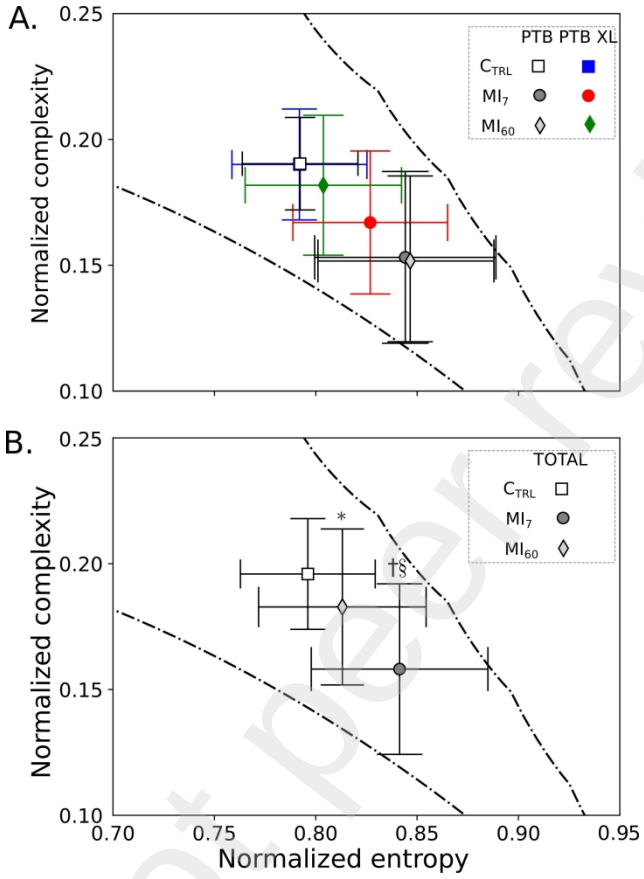


Figure 1: Graphics showing the $\overline{HC}_{ML}$ plane for $C_{T\,RL}$ and infarcted patients subsets for MI_7 and MI_{60} stages for PTB and PTB XL databases (in panel A.); and *Total* database (in panel B.). Results are presented as mean ± SD on both axes. C_{min} and C_{max} are plotted with dash-dotted lines.

Table 2 shows Sensitivity and Specificity, expressed as percentages, and AUC, expressed in non-dimensional units, for the $\overline{H}_{ML}$ and $\overline{C}_{ML}$ quantifiers and the $\overline{HC}_{ML}$ plane, for $C_{T\,RL}$ vs MI_7, $C_{T\,RL}$ vs MI_{60}, and MI_7 vs MI_{60}, when the *Total* database is considered.

Preprint not peer reviewed

This preprint research paper has not been peer reviewed. Electronic copy available at: https://ssrn.com/abstract=5349412

Groups		$\overline{H}_{ML}$	C_{ML}	$\overline{HC}_{ML}$
C_{TRL} vs. MI_7	Sens (%)	83	84	80
	Spec (%)	71	75	75
	AUC	0.79	0.82	0.80
C_{TRL} vs. MI_{60}	Sens (%)	67	67	66
	Spec (%)	60	59	60
	AUC	0.62	0.63	0.63
MI_7 vs. MI_{60}	Sens (%)	67	67	67
	Spec (%)	64	68	67
	AUC	0.68	0.71	0.70

Table 2: Sensitivity and specificity, expressed as percentages, and AUC, expressed in non-dimensional units, for the $\overline{H}_{ML}$ and $\overline{C}_{ML}$ quantifiers and the $\overline{\overline{HC}}_{ML}$ plane, for C_{TRL} vs MI_7, C_{TRL} vs MI_{60}, and MI_7 vs MI_{60}.

The reason the ML criterion is used is that it consolidates the results from each of the 12 ECG leads into a single criterion. In addition, in Figure 2, lead-by-lead detail is presented to show that both $\overline{H}$ and $\overline{C}$ exhibit statistically significant differences between the groups, including MI_7 and MI_{60}, when considering the *Total* database.

Preprint not peer reviewed

This preprint research paper has not been peer reviewed. Electronic copy available at: https://ssrn.com/abstract=5349412

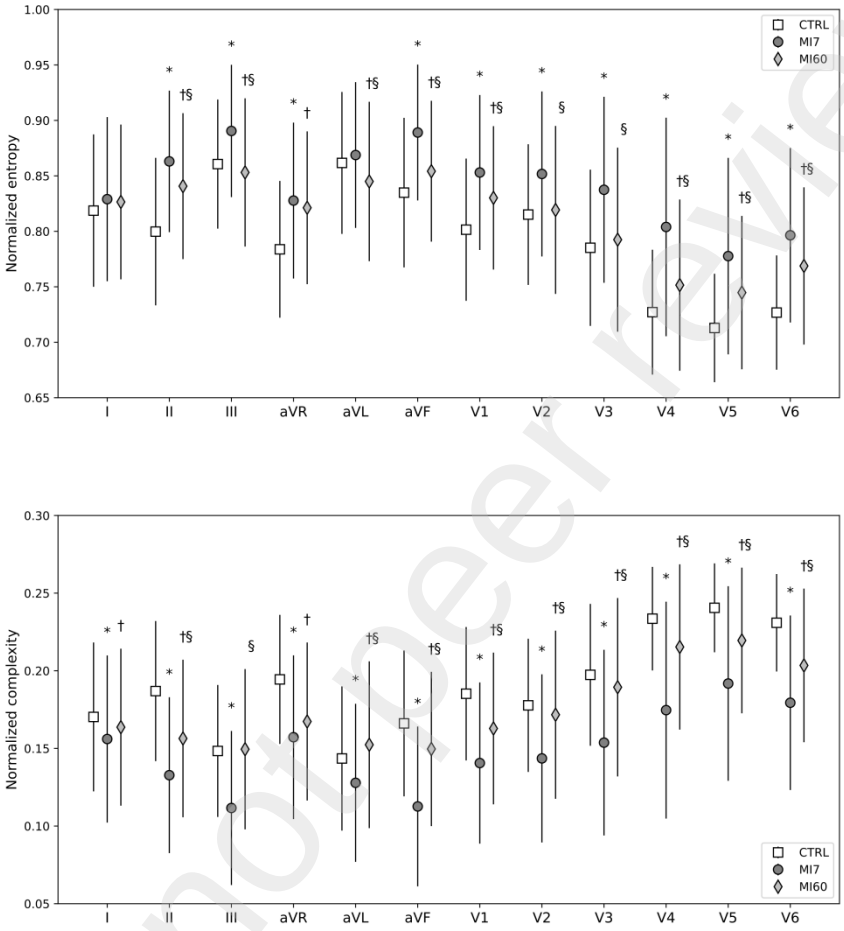


Figure 2: Graphics showing (above) normalized wavelet entropy $\overline{H}$ and (below) wavelet statistical complexity $\overline{C}$, both for each ECG leads. Results are presented as mean ± SD. $*$ indicate statistical significance differences between C_{TRL} and MI_7; † indicate statistical significance differences between C_{TRL} and MI_{60}; and § indicate statistical significance differences between MI_7 and MI_{60}.

4. Discussion

This study reinforces the use of Shannon entropy (H) and statistical complexity (C) indicators, derived from the Continuous Wavelet Transform (CWT), as non-invasive metrics for detecting alterations in cardiac

Preprint not peer reviewed

This preprint research paper has not been peer reviewed. Electronic copy available at: https://ssrn.com/abstract=5349412

electrical conduction. The results highlight significant differences between post-myocardial infarction patients in the MI_7 and MI_{60} phases and control subjects ($C_{T\,RL}$), analyzing micro-fragmentations of the QRS complexes (*μf QRS*) in public databases (PTB and PTB-XL) and their combination (*Total*). It is important to note that the indices employed combine the properties of entropy and complexity with the time-frequency localization of the wavelet transform. The benefits of these quantifiers are most apparent when applied to non-stationary signals, such as *μf QRS* that can appear in the ECG after a MI, and are defined from the relative energy set of frequency bands or wavelet resolution levels.

The fact that there are more men than women in the *Total* database in MI_7 and MI_{60} than in $C_{T\,RL}$ can be explained by the increased sample size when merging the data, which enhances the statistical power of the test, enabling the detection of smaller differences in sex proportions among the groups. Additionally, the intrinsic differences in proportions between each database may be amplified in the combined database, reflecting greater heterogeneity in the sex distribution.

Normalized wavelet entropy and wavelet statistical complexity provide key information about the underlying processes in the ECG. Entropy reflects the level of randomness in the signal, and its increase indicates more disorder and energy dispersion across various scales. On the other hand, wavelet complexity captures the correlation structure between signal components. In healthy subjects, electrical conduction is coordinated, whereas in post-infarction patients, it becomes erratic, decreasing electrical connectivity and affecting ventricular activation synchronization. During a MI, the signal shows increased randomness, increasing entropy, and a reduction in the correlation structure, decreasing complexity. This is observed in the results, where $\overline{H}_{ML}$ increased and $\overline{C}_{ML}$ decreased significantly in post-MI patients compared to controls. The $\overline{HC}_{ML}$ plane showed statistically significant differences among the studied groups, suggesting that the combined entropy and complexity indicators are useful for discriminating between healthy subjects and those in different post-MI phases. These findings confirm that metrics derived from the CWT can capture subtle alterations in cardiac electrical activity that may not be evident through classical ECG analyses. However, differences in discriminatory ability were observed depending on the database used: in the PTB-XL database, significant differences were detected among all groups, including MI_7 and MI_{60}, while no such differences were observed in the PTB database. When considering the *Total* database, the $\overline{H}_{ML}$ and $\overline{C}_{ML}$ indices, as well as the $\overline{HC}_{ML}$ plane, showed reasonable sensitivity and specificity values when discriminating among the groups, with

Preprint not peer reviewed

This preprint research paper has not been peer reviewed. Electronic copy available at: https://ssrn.com/abstract=5349412

areas under the curve (AUC) reaching up to 0.82 for $C_{T\,RL}$ vs. MI_7. Although the AUC values for $C_{T\,RL}$ vs. MI_{60} and MI_7 vs. MI_{60} were more modest, these results align with the expected differences in the characteristics of the studied groups.

The results suggest that the quantifiers H and C show significant differences between the studied groups, indicating that they capture morphological changes due to a reordering of wavelet scale energies that could be related to electrical alterations after MI. The presence of $\mu f\,QRS$ in the ECG may be associated with myocardial scarring, interstitial fibrosis, and subclinical myocardial damage because they are signals of electrical activity disturbances in the heart, often resulting from structural changes in cardiac tissue. Furthermore, the evolution of H and C values between MI_7 and MI_{60} suggests that structural reorganization of the post-MI could still be underway even months after the initial event. It is important to highlight that these changes do not necessarily reflect a homogeneous phenomenon but may depend on individual factors, such as infarction extent and the presence of comorbidities. Therefore, in practice, $\mu f\,QRS$ should be considered by combining different risk indicators. Other limitations of this study are related to the retrospective nature of the data and the imbalance in patient distribution between the analyzed groups, which could influence the interpretation of the results. Although the combination of the PTB and PTB-XL databases allowed for an expanded sample, the imbalance in favor of the $C_{T\,RL}$ group could affect the generalizability of the indicators. Additionally, the detection of $\mu f\,QRS$ through the quantifiers H and C requires further validation with prospective data and comparison with other methods.

For future research, we plan to extend the analysis to other databases, which could provide a more balanced distribution of the study groups. Although the PTB-XL database is larger than the PTB, both are imbalanced in favor of one group, which may affect the robustness of the results when combining the datasets. Having a more balanced database or including new patients, like the dataset used in [5], would help determine whether the proposed quantifiers can establish a clear threshold that allows for the unequivocal identification of infarct presence. We also aim to explore the combination of the proposed indicators with other features related to ECG morphology or rhythm, as well as machine learning algorithms to improve the detection and prediction of adverse events. In this context, we find it relevant to apply this methodology to other pathologies, such as Chagas cardiomyopathy, given the high prevalence of this disease in our region. The electrical conduction alterations associated with Chagas could be reflected

Preprint not peer reviewed

This preprint research paper has not been peer reviewed. Electronic copy available at: https://ssrn.com/abstract=5349412

in the proposed quantifiers, offering an additional tool for its early detection. Furthermore, the focus of the 2025 Computing in Cardiology Challenge on this topic highlights the relevance and potential of this line of research.

The study presents notable aspects, with one of the most significant contributions being the integration of two databases, PTB and PTB-XL, which offered a more representative sample. This combination enhanced statistical validity and the ability to generalize the results. In this context, the findings emphasize the importance of the proposed indicators to differentiate study groups, as evidenced by the high AUC values. This suggests that the indices capture key features of the analyzed phenomenon, such as changes in QRS morphology, reflected in the redistribution of energy in wavelet scales. Furthermore, the algorithms used to evaluate *μf QRS* are not computationally expensive, facilitating their implementation on standard ECG digital acquisition equipment. The codes used in this study can be downloaded from https://github.com/Yecaergi/Quantifying-Heartbeat-Micro-Fragmentations-Post-Myocardi git. These scripts enable the reproduction of the results presented in the manuscript.

This study provides evidence that entropy and complexity indicators derived from CWT are promising tools for evaluating morphological changes in the QRS complex of post-MI patients. These findings support their usefulness in *μf QRS* analysis and highlight their potential application in clinical and medical research settings.

Acknowledgment

Competing interests: The authors declare no competing interests.

Ethical approval: Not required.

Funding: This research was funded by Universidad Tecnológica Nacional, Facultad Regional Buenos Aires, under projects ICTCBA8666TC and ICUTIBA6564TC; and a CONICET fellowship.

References

[1] M. Koivunen, J. Tynkkynen, N. Oksala, M. Eskola, J. Hernesniemi, Incidence of sudden cardiac arrest and sudden cardiac death after unstable angina pectoris and myocardial infarction, American Heart Journal, Volume 257 (2023) 9-19. https://doi.org/10.1016/j.ahj.2022.11.009.

Preprint not peer reviewed

This preprint research paper has not been peer reviewed. Electronic copy available at: https://ssrn.com/abstract=5349412

[2] G. Li, S. Liu, J. Jin, K. Ding, C. Qian, Risk Factors Associated with the Incidence of Ventricular Arrhythmias Complicating Acute Myocardial Infarction and Prognosis Analysis, Journal of NanomaterialsVolume (2021). https://doi.org/10.1155/2021/9985899.

[3] K. Hnatkova, I. Andršová, T. Novotný, A. Britton, M. Shipley, B. Vandenberk, D.J. Sprenkeler, J. Junttila, T. Reichlin, S. Schlögl, Marc A. Vos, T. Friede, A. Bauer, H.V. Huikuri, R. Willems, G. Schmidt, M.R. Franz, C. Sticherling, M. Zabel, M. Malik, QRS micro-fragmentation as a mortality predictor, European Heart Journal (2022) 00, 1–15. https://doi.org/10.1093/eurheartj/ehac085.

[4] P. Xiong, SM-Y Lee and G. Chan, Deep Learning for Detecting and Locating Myocardial Infarction by Electrocardiogram: A Literature Review, Front. Cardiovasc. Med. 9:860032 (2022). https://doi.org/10.3389/fcvm.2022.860032.

[5] G.A. Tadesse, J. Chen, T. Zhu, H. Javed, K. Weldemariam, Y. Liu, J. Liu, DeepMI: Deep multi-lead ECG fusion for identifying myocardial infarction and its occurrence-time, Artificial Intelligence In Medicine 121, 102192 (2021). https://doi.org/10.1016/j.artmed.2021.102192.

[6] K. Hnatkova, I. Andršová, O. Toman, P. Smetana, K.M. Huster, M. Šišáková, P. Barthel, T. Novotný, G. Schmidt, M. Malik, Spatial distribution of physiologic 12-lead QRS complex, Sci Rep (2021) 11:4289. https://doi.org/10.1038/s41598-021-83378-8.

[7] E.R. Valverde, G.V. Clemente, P.D. Arini, and V. Vampa, Wavelet-based entropy and complexity to identify cardiac electrical instability in patients post myocardial infarction, Biomedical Signal Processing and Control, Vol. 69, Article 102846 (2021). https://doi.org/10.1016/j.bspc.2021.102846.

[8] E.R. Valverde, V. Vampa, O.A. Rosso, P. Arini, Spatio-Temporal Analysis of Acute Myocardial Ischaemia Based on Entropy–Complexity Plane, Entropy (2025) 27, 8. https://doi.org/10.3390/e27010008.

[9] L. Sörnmo, P. Laguna, Bioelectrical signal processing in cardiac and neurological applications, Elsevier Academic Press, 2005.

[10] J. Mart´ınez, R. Almeida, S. Olmos, A. Rocha, P. Laguna, A wavelet-based ECG delineator: evaluation on standard databases, IEEE Trans. Biomed. Eng. 51 (4) (2004) 570–581. doi: 10.1109/TBME.2003.821031.

Preprint not peer reviewed

This preprint research paper has not been peer reviewed. Electronic copy available at: https://ssrn.com/abstract=5349412

[11] S. Mallat, A Wavelet Tour of Signal Processing. The Sparse Way, third ed., Academic Press, 2009.

[12] J. Lin, Divergence measures based on the Shannon entropy, IEEE, Transactions on Information Theory, 37(1) (1991) 145-151. doi: 10.1109/18.61115.

Preprint not peer reviewed

This preprint research paper has not been peer reviewed. Electronic copy available at: https://ssrn.com/abstract=5349412